JOURNAL OF CHEMICAL INFORMATION AND MODELING

Article

pubs.acs.org/jcim

Discovery of a Novel Selective PPARγ Ligand with Partial Agonist Binding Properties by Integrated *in Silico/in Vitro* Work Flow

Irene Kouskoumvekaki,*[,†] Rasmus K. Petersen,[‡,§] Filip Fratev,[†,∥] Olivier Taboureau,[†,⊥] Thomas E. Nielsen,[#,▽] Tudor I. Oprea,[†,○] Si B. Sonne,[§] Esben N. Flindt,[‡,§] Svava Ósk Jónsdóttir,[†,◆] and Karsten Kristiansen*[,§]

[†]Center for Biological Sequence Analysis, Department of Systems Biology, Technical University of Denmark, DK-2800 Kgs. Lyngby, Denmark

[‡]BioLigands, Science Park, 5230, Odense, Denmark

[§]Department of Biology, University of Copenhagen, Ole Maaløes Vej 5, DK-2200, Copenhagen, Denmark

[∥]Micar 21 Ltd., 34B Persenk Str., 1407, Sofia, Bulgaria

[⊥]UMR-S973, MTi, University Paris Diderot, F-75013 Paris, France

[#]Department of Chemistry, Technical University of Denmark, DK-2800 Kgs. Lyngby, Denmark

[▽]Singapore Centre on Environmental Life Sciences Engineering, Nanyang Technological University, Singapore 637551

[○]Translational Informatics Division, Department of Internal Medicine, MSC09 5025, University of New Mexico School of Medicine, Albuquerque, New Mexico 87131, United States

[◆]Department of Toxicology and Risk Assessment, National Food Institute, Technical University of Denmark, Mørkhøj Bygade 19, DK-2860 Søborg, Denmark

Supporting Information

ABSTRACT: Full agonists to the peroxisome proliferator-activated receptor (PPAR)γ, such as Rosiglitazone, have been associated with a series of undesired side effects, such as weight gain, fluid retention, cardiac hypertrophy, and hepatotoxicity. Nevertheless, PPARγ is involved in the expression of genes that control glucose and lipid metabolism and is an important target for drugs against type 2 diabetes, dyslipidemia, atherosclerosis, and cardiovascular disease. In an effort to identify novel PPARγ ligands with an improved pharmacological profile, emphasis has shifted to selective ligands with partial agonist binding properties. Toward this end we applied an integrated *in silico/in vitro* workflow, based on pharmacophore- and structure-based virtual screening of the ZINC library, coupled with competitive binding and transactivation assays, and adipocyte differentiation and gene expression studies. Hit compound **9** was identified as the most potent ligand (IC_{50} = 0.3 μM) and a relatively poor inducer of adipocyte differentiation. The binding mode of compound **9** was confirmed by molecular dynamics simulation, and the calculated free energy of binding was −8.4 kcal/mol. A novel functional group, the carbonitrile group, was identified to be a key substituent in the ligand−protein interactions. Further studies on the transcriptional regulation properties of compound **9** revealed a gene regulatory profile that was to a large extent unique, however functionally closer to that of a partial agonist.

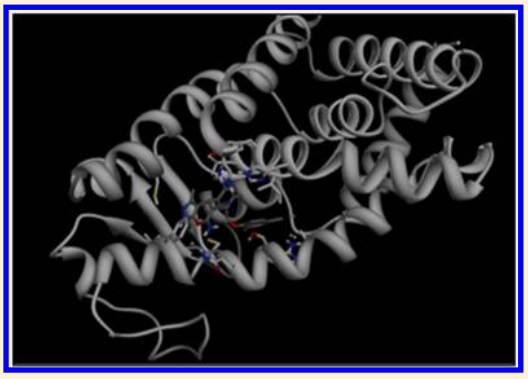

INTRODUCTION

Peroxisome proliferator-activated receptors (PPARs) are transcription factors that belong to the nuclear receptor family. The three PPAR subtypes PPARα, PPARδ, and PPARγ play an important role in glucose and lipid homeostasis.[1] The PPARγ subtype is most highly expressed in adipose tissue, and its agonists increase adipocyte differentiation, enhance insulin sensitivity, and improve lipid profiles.[2−4] Natural ligands of PPARγ are fatty acids as well as eicosanoids. These include linoleic acid, linolenic acid, arachidonic acid, eicosapentaenoic acid, and metabolites of the 15-lipoxygenase pathway such as 9-HODE and 13-HODE.[5]

PPARγ ligands are, primarily based on their activity in transactivation assays, categorized into three groups: full agonists, partial agonists, and antagonists. Among a large variety of synthetic PPARγ full agonists are thiazolidinediones (TZDs) and some nonsteroidal anti-inflammatory drugs. TZDs have been used in clinical practice to treat type II diabetes for

Received: December 20, 2012
Published: February 24, 2013

many years and have been shown to lower blood glucose levels and improve insulin sensitivity.[6] However, despite their excellent potencies, administration of TZDs has been associated with severe side effects such as fluid retention, weight gain, cardiac hypertrophy, and hepatotoxicity.[7,8] Troglitazone was withdrawn from therapeutic use due to liver toxicity and Farglitazar failed to pass phase III clinical trials due to the emergence of peripheral edema. Since 2011, Rosiglitazone has been withdrawn from the European market following incidents of fluid retention, heart failure, weight gain, and cardiovascular risks. Pioglitazone is currently in clinical practice despite being also linked to controversial side effects including an increased risk of cardiovascular related death.

Weight gain associated with PPARγ agonist activity is due to the stimulation of adipocyte differentiation.[6] In an effort to overcome this side effect, researchers have looked into the development of dual and pan PPAR agonists. In contrast to selective PPARγ agonists, PPARα/γ dual agonists combine the insulin sensitizing effect of PPARγ agonists with the beneficial lipid modulating activities of the PPARα agonists.[4] Similarly, PPARγ/δ dual agonists provide dual control of glucose and lipid metabolism via exploiting the propensity of PPARδ to improve insulin sensitivity and stimulate fatty acid oxidation.[9] Thus, it was believed that a PPARα/γ dual or PPAR$\alpha/\gamma/\delta$ pan agonist would be an all-in-one therapy for type II diabetes, correcting insulin resistance and lipid imbalances associated with metabolic syndrome simultaneously, and might overcome some of the side effects of a selective PPARγ agonist. On the basis of this concept, several PPARα/γ-dual and PPARR$\alpha/\gamma/\delta$-pan agonists were developed and tested in the clinic; however, they were soon abandoned because of concerns over cardiovascular safety and propensity to cause cancer on prolonged administration.[10]

At the same time, recent identification of novel partial agonists with no or low adipogenic potential suggests that this effect might be primarily restricted to full agonists.[11] The reduced adipogenic activity of partial agonists is probably related to the induction of alternative structural conformational changes of the receptor, leading to recruitment of a differential set of cofactors and/or changed exposure to posttranslational modifications. Thus, partial agonists are expected to retain full insulin sensitizing effects without carrying along the unwanted side-effects.[12,13] One such partial agonist, Balaglitazone, is the first partial agonist in phase III clinical trials.[14] Balaglitazone activates PPARγ 50% less than full agonists and has shown promising results in relation to glucose levels improvement and absence of fluid and fat accumulation.

In view of these developments, novel selective PPARγ ligands with partial agonist binding properties would be advantageous not only as candidates for the treatment of type II diabetes but also as chemical probes for the elucidation of the biological function of PPARγ and its potential role in the treatment of other diseases, such as obesity.[15] Toward the goal of identifying new ligand molecules that bind selectively to PPARγ in a partial agonist mode, we designed an *in silico/in vitro* workflow based on pharmacophore-based and structure-based virtual screening (VS) of the ZINC library, combined with competitive binding and transactivation assays. The selectivity and binding mode of the obtained hits were further evaluated via docking, molecular dynamics, and MM-PBSA and MM-GBSA free energy of binding calculations. Finally, the active compounds were analyzed with respect to partial versus full agonist activity by adipocyte differentiation and gene expression.

RESULTS AND DISCUSSION

The integrated *in silico/in vitro* workflow is shown in Figure 1. Pharmacophore-based virtual screening was performed on the ZINC library using MOE v. 2007.09. 256 hits were further subjected to high throughput docking with Autodock 4.1. 106 compounds that passed the docking filter were inspected visually, and 15 were selected based on docking score, availability, structural diversity, and low risk of toxicity. Competitive binding and transactivation assay experiments on the 15 compounds showed that 11 of them were active against PPARγ, while 6 were also able to stimulate PPARγ-mediated transactivation. The 6 hits were further tested for *in vitro* adipocyte differentiation. Their binding mode on PPARγ and their selectivity toward all three PPAR subtypes were analyzed *in silico*, using Autodock 4.1, while the binding mode of the best hit was studied in more detail with Molecular Dynamics (MD) using AMBER 11. Finally, the ability of the best hit to regulate gene expression was evaluated *in vitro*.

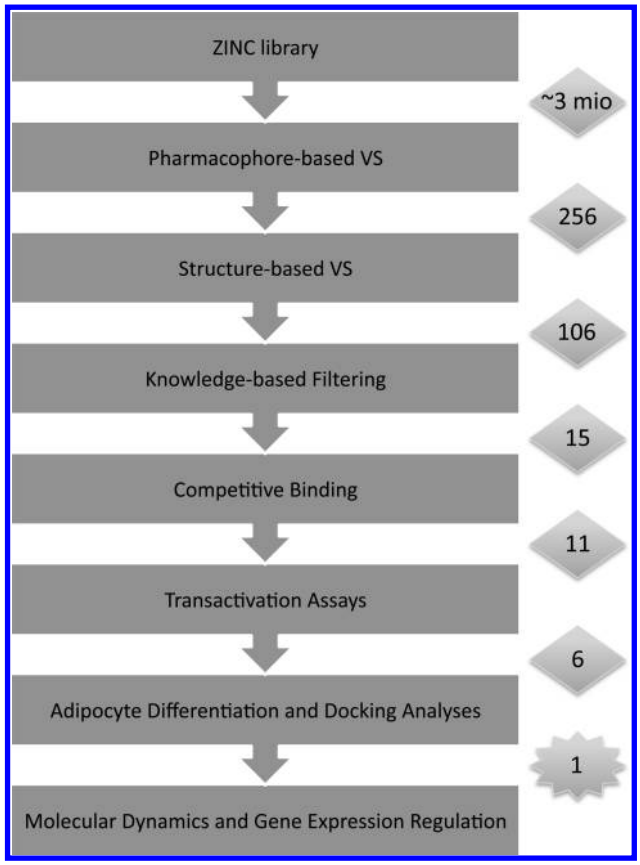

Figure 1. Schematic view of the integrated *in silico/in vitro* workflow. Pharmacophore-based virtual screening was performed on the ZINC library, and 256 hits were further subjected to high throughput docking. 106 compounds that passed the docking filter were inspected visually, and 15 were selected based on availability, structural diversity, and low risk of toxicity. Competitive binding and transactivation assay experiments on the 15 compounds showed that 11 of them were active against the PPARγ receptor, while 6 were also able to stimulate PPARγ-mediated transactivation. The 6 hits were further tested for *in vitro* adipocyte differentiation. Their binding mode on PPARγ and their selectivity toward all three PPAR subtypes were analyzed *in silico*, while the binding mode of the best hit was studied in more detail with molecular dynamics simulation. Finally, the ability of the best hit to regulate gene expression was evaluated *in vitro*.

dx.doi.org/10.1021/ci3006148 | J. Chem. Inf. Model. 2013, 53, 923−937

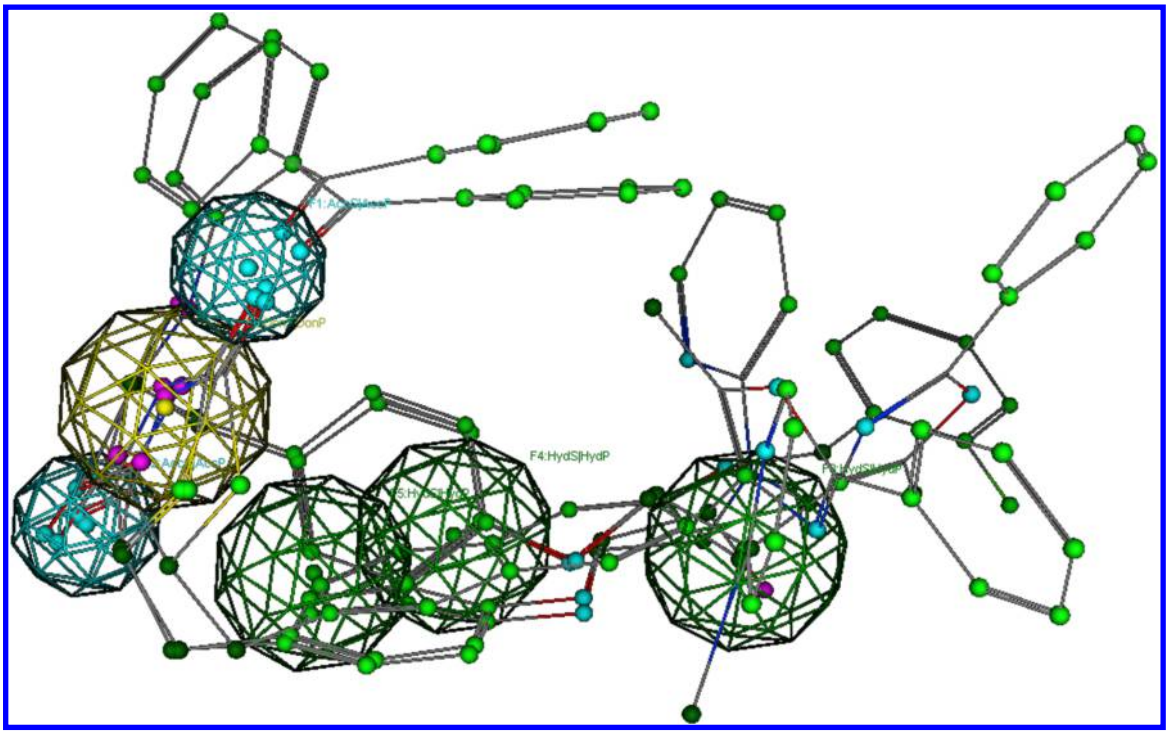

Figure 2. 6-point pharmacophore model for PPARγ ligands superimposed on the structures of the 5 active compounds from the training set. In MOE, pharmacophoric features are represented by a point encased in a sphere.[26] The spheres depict the location tolerance allowed during virtual screening. (F1, F2 radii: 1.0 Å, F3−F6 radii: 1.4 Å) Blue: hydrogen-bond acceptors, Yellow: hydrogen-bond donor, Green: hydrophobic regions.

Pharmacophore-Based Virtual Screening. In order to elucidate the most optimal common pharmacophore that is shared by a set of PPARγ ligands, each ligand was allowed the flexibility to take other energetically favorable conformations than the one that was captured in the protein−ligand complex stored in the Protein Data Bank (PDB).[16] We, thus, chose not to restrict our model to the one reported bioactive conformation of each PPARγ agonist for the development of the pharmacophore model. We followed this strategy because we have observed that the same ligand can adopt different bioactive conformations in a complex with PPARγ, as can be seen in the 1ZGY.pdb[17] and 2PRG.pdb[18] complexes with Rosiglitazone. At the same time, the binding pocket of PPARγ is able to adapt to the conformation of the ligand by shifting side chains of residues in the cavity and thereby modifying the volume of armI. This can be seen in the 1K74.pdb[19] and 2F4B.pdb[20] complexes of PPARγ with ligands GW409544 and EHA, respectively. Adding to this, there is support from previous studies that such a ligand-based pharmacophore approach is more successful in retrieving selective PPARγ ligands than an approach based on PPARγ ligand−protein complexes.[21]

A 6-point pharmacophore model was obtained, which consisted of two hydrogen bond acceptors, one hydrogen bond donor, and three hydrophobic spheres (see Figure 2). The model matched five of the seven active compounds (with the exception of Telmisartan and RWJ-348260) and none of the inactive compounds in the training set. In order to prioritize the best hits and reduce the number of false positives from the ZINC database, volume and pharmacophoric radii constraints were added to the original model. The volume constraint was designed to take the shapes of all seven active compounds of the training set into account, ensuring that larger molecules were not going to be accepted by the model. The radii were reduced to 0.8 Å for the hydrogen-bond acceptor features, 1.0 Å for the hydrogen-bond donor feature, and to 1.1 Å for the hydrophobic features, which were the minimum values for retrieving the five active compounds matched by the original model. When the constrained model was used for the virtual screening of the ZINC database, it retrieved 256 hit compounds.

Structure-Based Virtual Screening. The binding modes of the 256 compounds selected with the pharmacophore-based screening were explored with the docking procedure described below. Compounds with Autodock docking score ΔG_{intr} ($\Delta G_{intr} = \Delta G - \Delta G_{torsions}$, i.e. the torsion scoring term was excluded) less negative than a threshold value of −10 kcal/mol passed the docking screen, and the remaining compounds were discarded. The threshold value was identified by analyzing the docking scores of the 19 compounds in the docking test set against their transactivation values. All 14 compounds that were defined as actives had $\Delta G_{intr} < -10$ kcal/mol, and four of the five compounds defined as inactive had $\Delta G_{intr} \geq -10$ kcal/mol, indicating that the Autodock docking score for a given compound may have some relevance with respect to its transactivation. For each compound, the pose giving the most negative docking score from the top group of most populated ligands was used. Based on the above procedure 106 of the 256 compounds passed the docking screen.

Furthermore, the binding modes of the compounds that passed the docking screen were examined by visual inspection. In particular it was seen that carbonitrile (CN), sulfonyl (SO_2), and barbituric groups interacted closely with the key residues in armI of the PPARγ binding pocket. Along these lines, the ligands were divided according to the functional groups mentioned above, and the compounds with higher docking score from these groups were selected.

dx.doi.org/10.1021/ci3006148 | J. Chem. Inf. Model. 2013, 53, 923−937

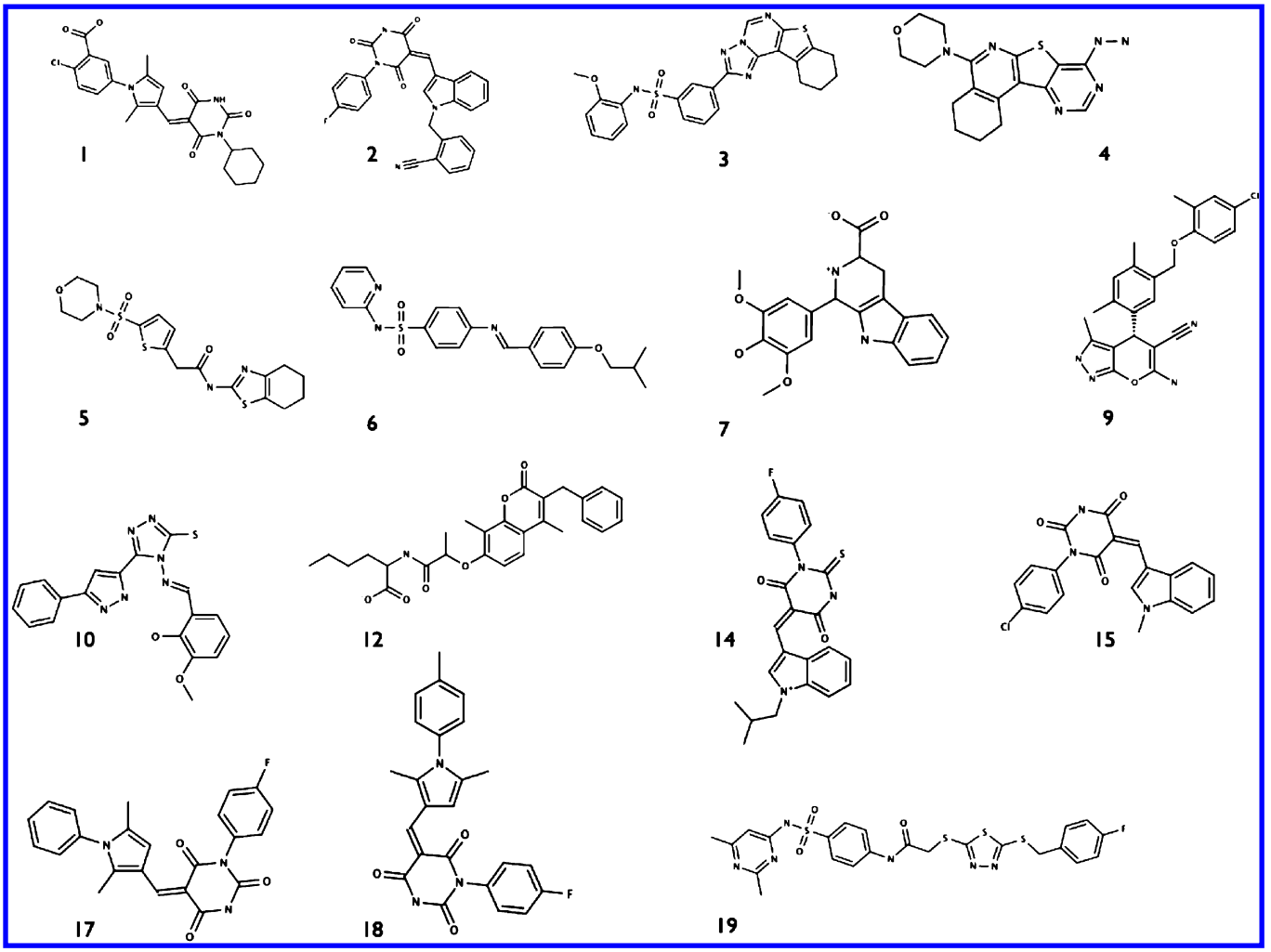

Figure 3. The 15 hits from the virtual screening of the ZINC library that were selected for experimental testing.

Knowledge Based Filtering. A subset of 15 compounds was selected for *in vitro* testing according to the criteria given in the methods section, with four of the compounds being analogues to compound **2**. Compounds containing sulfonyl, carbonitrile, and barbituric groups were identified to have strong interactions with key residues and were thus appropriately represented within the selected subset. In addition, a diverse set of compounds containing interesting scaffolds was selected.

We principally aimed to avoid potentially reactive and/or toxic compounds during the selection process. However, although both the barbituric and carbonitrile groups occasionally have such undesirable properties, several compounds containing these groups showed very strong interactions with key residues within armI of the PPARγ binding pocket and had relatively high docking scores. Therefore, several compounds containing these groups were included in the subset.

As shown in Figure 3, compounds **1** and **2** contain a barbituric group, while compound **2** contains a carbonitrile group as well, compounds **3**, **5**, **6**, and **19** contain a sulfonyl substructure, compound **9** has a carbonitrile group, and compounds **7** and **12** have a carboxyl group. Furthermore, all four analogues of compound **2**, namely compounds **14**, **15**, **17** and **18**, contain a barbituric group.

Competitive Binding and Transactivation Assays. As discussed above, 15 commercially available compounds were selected for biological testing. Eleven of these compounds dose-dependently displaced a labeled PPAR ligand in the applied TR-FRET *in vitro* competitive binding assay. Potency of binding as compared with known PPAR ligands ranged from low affinity, as for compound **17** with IC_{50} = 67 μM, to fairly high affinity, as observed for compound **9** (IC_{50} = 0.3 μM) (Table 1). Rosiglitazone displacement was measured to IC_{50} of 58 nM in this assay, in agreement with previously reported affinities.[22] Further, to examine receptor binding at a more functional level we analyzed the compounds' ability to induce transcriptional activation in a cell-based transactivation assay. Six compounds were found to stimulate PPARγ-mediated transactivation, all with efficiencies much lower than Rosiglitazone (Table 1). However, we cannot exclude that some of the compounds did not reach saturating concentrations in the transactivation setup, and thus from these experiments we are not able to conclude whether the observed low efficiencies are signs of partial agonism. Although there was no apparent correlation between *in vitro* binding affinity and cell-based transactivation efficiency, all compounds displaying transactivating potential were also found to bind to the receptor. As several relatively potent binders (compounds **6**, **10**, and **14**) did not induce transcriptional activation, we speculated whether these compounds behaved as antagonists. However, none of these compounds were able to antagonize Rosiglitazone induced transactivation (data not shown).

dx.doi.org/10.1021/ci3006148 | *J. Chem. Inf. Model.* 2013, 53, 923−937

Table 1. PPARγ Activity of Hit Compounds[a]

		PPARγ	
compound	ZINC code	IC_{50} (μM)	transactivation
1	ZINC02065569	45	-
2	ZINC00853309	0.9	11.3%
3	ZINC03208153	-	-
4	ZINC04795081	-	-
5	ZINC03374787	1.2	5.8%
6	ZINC06409377	12	-
7	ZINC00754304	-	-
9	ZINC00650578	0.3	13.3%
10	ZINC09359214	4.2	-
12	ZINC02154374	6.0	13.9%
14	ZINC00667028	3.1	-
15	ZINC00757983	18	5.2%
17	ZINC00853249	67	4.4%
18	ZINC00853261	-	-
19	ZINC03364455	26	-
Rosiglitazone		0.058	100%

[a]IC_{50} values for binding to the PPARγ-LBD were calculated from a competitive in vitro binding assay (see the Methods section). Stimulation of PPARγ-LBD transcriptional activity was measured using a cell-based Gal4-reporter system (see the Methods section). Compounds were tested up to a concentration of 100 μM (compounds **5** and **6**) or to the highest concentration compatible with the assay (compound **9** up to 10 μM and remaining compounds up to 50 μM). Transcriptional activity was calculated as fold activation above vehicle background and with Rosiglitazone (full agonist) induced activation set to a 100%.

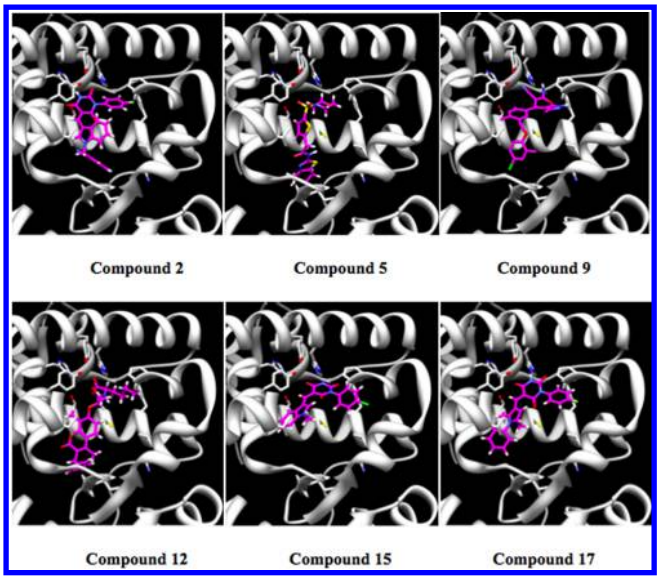

Figure 4. Ligand−protein interactions of the six hits docked into PPARγ (1K74). Each ligand is shown in magenta. Important residues involved in the ligand binding pocket are in stick. The protein is represented in cartoon.

It was indeed observed that most of the selected compounds showed PPARγ binding activity, with the exception of compounds **3**, **4**, **7**, and **18**. Thus the hit rate among the tested compounds can be considered high by any standards, with three compounds, namely **2**, **5**, and **9** displaying potency in the low micromolar range. We believe that the success of our approach is largely due to both the set constraints of the pharmacophore model and the chosen docking model. We were able to capture important binding properties among known PPARγ agonists and identify new compounds that bind to PPARγ. Moreover, the docking analysis was helpful for implementing an additional filter for reducing potential false positive ligands and the less likely binders. However, no strong correlation was found between docking score and binding affinity for the compounds tested, confirming previous statements that scoring functions are approximate values for binding energies that vary between software, rather than quantitative indicators of binding affinity.[23,24]

Evaluation of PPARγ Binding Mode. To evaluate the binding mode of the six hits that showed positive transactivation in PPARγ, we docked them into the crystal structure with PDB ID: 1K74. The protein residues that interact with the ligands and the nature of these interactions were identified as shown in Figure 4 and Figure S2 in the Supporting Information.

Compound **9** displayed the highest binding activity (IC_{50} = 0.31 μM), see Table 1. Docking of compound **9** in PPARγ showed interactions with key residues located in the activation function domain (AF-2) within armI of the PPARγ binding pocket. The carbonitrile group was seen to interact with His323, Tyr327, His449, and Tyr473 and make H-bonds with the latter (see Figures 4 and S2). The phenyl-substituted pyranopyrazole group was stabilized with several hydrophobic interactions with Phe285, Leu330, Ile341, and Phe363. The amino group was stabilized through an H-bond interaction with the carbonyl group of Phe282, while the NH substituent formed a hydrogen bond with Ile281. The attached aromatic group was stabilized by interactions with Cys285, Ile326, and Tyr327. It should be noted that the carbonitrile group fits much better into the key residue pocked (armI) than the phenyl halogen, which is known to interact with PPARγ armI residues.[13] Considering the role of the carbonitrile group, one can conclude that the CN has been identified as a novel key substituent that shows strong interactions with the key PPARγ residues. Further optimization of the position of the carbonitrile group could possibly increase the biological activity.

Compound **2** has a binding activity of 0.89 μM. This molecule contains a barbituric acid group and was also stabilized with the same network of residues, His449, Met364, and Tyr327, as described previously for compound **9**. In addition, the indole group was stabilized with hydrophobic residues in the hydrophobic pocket. The carbonitrile group in compound **2** displayed a close contact and strong interaction with Arg288 that might contribute to activity too. In agreement to a recent study suggesting the involvement of the barbituric acid group in the interaction with residues from AF-2, all poses from our docking procedure confirmed the formation of this network.[24]

Compound **5**, with a binding activity of 1.2 μM, depicted a similar binding mode. The sulfonyl and morpholine groups reached the AF-2 helix 12. The sulfonyl group formed H-bonds with Ser289 and Tyr327 and showed stronger interactions with His323 as well, and the morpholine group interacted with His449 and Tyr473. Additionally a hydrophobic contact with Phe282 of armIII has been identified. The benzothiazol part of the molecule was stabilized in the armII region in a similar position as the phenyl-1−3-oxazol group observed in the 3D structure of PPARγ in a complex with GW409544.

Compound **12** depicted interactions with His449, Tyr473, Ser289, and His323 of PPARγ, and the carboxyl acid group formed H-bonds with His323 and Tyr473 in the armI pocket.

dx.doi.org/10.1021/ci3006148 | J. Chem. Inf. Model. 2013, 53, 923−937

The alkyl chain was placed in armIII and interacted with Phe282, Phe363, and Val339. The oxochromen was stabilized with hydrophobic interactions with Leu330, Met364, and Cys285.

Compounds **2**, **15**, and **17** display structural similarities and also similar binding modes in PPARγ, but compound **15** and compound **17** showed 15- and 55-fold loss of activity compared to compound **2**, respectively. According to our docking analysis, both compounds **2** and **15** interacted with the key residues Ser289, His323, Tyr473, and His449 via the barbituric group, and the phenyl halogen interacted with Phe282 and Phe363. The difference in activity is most likely due to the fact that the barbituric group was not fitted deep enough into the armI cavity and that only one H-bond with Tyr473 was observed (Figure 4). The orientation for pi-pi stacking with Tyr327 was not so favorable compared to compound **2** too.

The docking studies of compounds **15** and **17** revealed similar binding modes, where the barbituric acid of these ligands was kept in armI through interactions with His449. Also an H-bond with Tyr473, constraining the indole in the hydrophobic pocket, was seen for both compounds. The 4-fold difference in activity between compounds **15** and **17** could originate from the presence of a dimethyl group on the pyrrol instead of a methyl group connected to the indole. Recently, a study performed on benzimidazole derivatives confirmed the importance of the methyl groups at the benzimidazole core for full agonistic activity.[1] The negative influence of Arg288, as identified in the MD simulations of compound **9** (see below), could also explain the loss of activity for compound **17**. Moreover, the aromatic ring of compound **15** was in closer contact with Tyr327 and presumably the pi-pi stacking has a significant effect contributing to better activity.

Compound **1**, which has a barbituric group as well, but not a phenyl-substituted ring attached, showed significant decrease in PPARγ binding activity. The importance of the phenyl halogen substituent was proven for various series of ligands,[13] and our results showed that the barbituric group of compound **1** was not able to interact with His449 and Tyr473 but only with Ser289. In general, different substituents surrounding the barbituric scaffold seemed to influence the ligand's binding mode.

Compound **6** contains a sulfonyl group, like compound **5**, which was seen to interact with PPARy armI residues. However the attached substituent that interacted with armIII residues might contribute to the significant decrease in activity seen for this compound, compared to compound **5**.

Compound **10** has a unique structure within our set and showed a good PPARγ binding activity (IC_{50} = 4.2 μM) but no transactivation. The triazole derivative group interacted with the key residues His449, Tyr473, Ser289, and His323, but no hydrogen bonds were observed, which supports the *in vitro* results.

We did not profit from taking flexible residues into consideration during both our docking analysis above and the docking screen. Instead we selected among various PDB structures the protein conformation that gave the best reproduction of available cocrystallized ligand structures by docking them into the available crystal protein structures. In this way the possible rotational degree of freedom was reduced, and docking accuracy was improved. Importantly a refinement of the docking protocol has been obtained by variation of many docking parameters in order to obtain the most appropriate values for PPARγ. Surprisingly, to our knowledge such an approach has not been reported before in the literature.

Indeed the constructed docking protocol cannot reproduce conformational changes of the protein in all cases. Thus to describe this and to determine the free energy of binding, we ran MD simulation for the most active compound in terms of IC_{50}, compound **9**. In addition, we used MD to verify the identified interactions between one of the ligands (compound **9**) and the residues within PPARγ. We believe that docking results can provide some initial understanding of the observed transcriptional activity of the ligands. Furthermore, long-time MD simulations with enhanced sampling approach would be helpful to describe the conformational dynamics of the obtained above complexes, and to reveal the nature of observed biological activity and stability of the helix 12 in greater detail. Such studies are, however, outside the scope of this paper.

Detailed MD Study of Compound 9. To understand the binding mode and dynamics of the most active hit more precisely and to reveal the role of the carbonitrile group, a 10 ns MD simulation has been performed, and the free binding energy of compound **9** was calculated by the MM-PBSA method. Further, an assessment of the protein residues contribution to the binding energy was evaluated by the MM-GBSA decomposition approach.

Supplementary Figures S3 and S4 show RMSD errors of the whole complex, compound **9** separately, and the predicted B-factors of the PPARγ residues, respectively. The complex reached a good convergence after the calibration step and remained stable during production run. All free binding energy evaluations were performed based on the data obtained after 2.0 ns time of the production run. The MM-PBSA calculation gave an enthalpy contribution of -36.9 ± 2.1 kcal/mol, while the entropy contribution was -28.5 ± 2.4 kcal/mol. Thus, the calculated free energy of binding was -8.4 kcal/mol, which is close to the obtained experimental value. The van der Waals term was predominant, with nearly four times higher contribution than the electrostatic one. The calculated solvation energy indeed contributed unfavorably with a value of 28.2 ± 1.3 kcal/mol.

Figure 5 illustrates the binding mode of compound **9** according to the MD simulation by averaging over the last 5 ns structures, and Figure 6 shows the contribution of all protein residues to the total free binding energy (only the enthalpy contribution) of the ligand−protein complex calculated by the MM-GBSA decomposition method. In consistence with the docking results, only the carbonitrile group interacted and formed hydrogen bonds with the key residues His323, His449, and Tyr473. The average distances between the carbonitrile N atom and the His323, His449, and Tyr473 residues were 3.8 Å, 4.0 Å, and 4.1 Å, respectively. These distances varied significantly during the simulation time in such way that formation of H-bond between these residues and the CN substituent occurred only 49%, 39%, and 38% of the simulation time, respectively, i.e. it was statistically impossible to identify a stable conformation. Thus according to the MD simulation, we could conclude that compound **9** cannot effectively stabilize the armI key residues, in particular Tyr473 of helix 12, which in turn might explain the observed partial agonism. These findings were supported by the calculated MM-GBSA energies. Significant interactions were identified between the carbonitrile group and His323 of helix 4 (enthalpy contribution of about -3 kcal/mol to the free energy) and with His449-Tyr473 pair (enthalpy contribution of about -2.5 − -3 kcal/mol to the free

dx.doi.org/10.1021/ci3006148 | J. Chem. Inf. Model. 2013, 53, 923−937

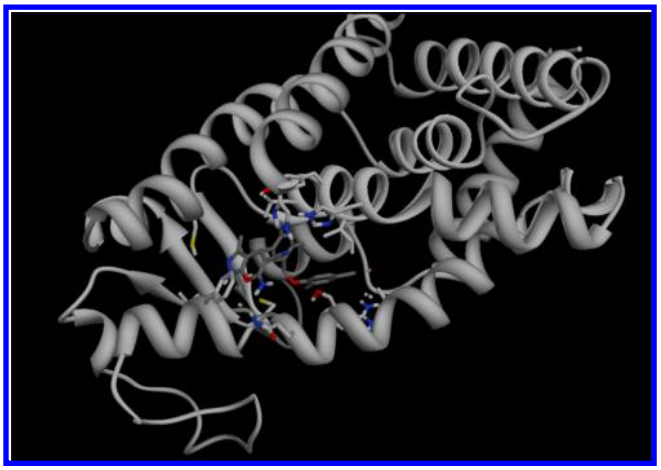

Figure 5. Binding mode of compound **9** in the PPARγ binding pocket based on averaged 8 ns MD simulation snapshot. The ligand is marked in dark gray. Favorable contacts with His323, His449, Phe282, and Arg288 are visible (see text for details). Water molecules are presented as white and red dots. The protein is represented in cartoon.

energy). These data suggest that compound **9** swings between the H4 and H11 helices and interacts relatively weaker with helix 12. Indeed such dynamics of the ligand are likely to destabilize the interactions with H12, presumably not allowing an effective coactivator interaction with the AF-2 surface. This behavior provides an additional support that might explain the observed partial agonism and indicates that the MD simulations can be helpful in revealing the mechanism of action. It should be noted that the above energies represent the contribution of only the CN substituent of compound **9** and not the remaining parts of the molecule. Thus, these results strongly suggest that the carbonitrile group is a new "lead" substituent that can fit between and effectively interact with the key PPARγ residues in armI. According to the above results, we speculate that an insertion of a second donor or acceptor group might additionally stabilize the interactions with the His449-Tyr473 and His323-Tyr327 pairs and thereby lead to increased agonist activity compared to compound **9**.

In summary, three protein residues that mainly interact with compound **9** were identified by the MM-GBSA methods, and total binding free energy of −43.5 ± 2.8 kcal/mol (only the enthalpy term) was calculated (Figure 6). In addition to the interactions of the carbonitrile group discussed above, the amino group of phenyl-pyranol[2,3-c]pyrazole forms a stable and strong H-bond with the backbone oxygen of Phe282 (average distance 2.86 ± −0.18 Å and 100% lifetime during the simulation). It is also likely that π−π stacking occurs between phenyl-pyranol[2,3-c]pyrazole and Phe282. The latter had a contribution of −5.61 kcal/mol to the binding energy/enthalpy of compound **9** within the ligand binding domain of PPARγ. Ile281, Leu330, Phe363, and Met364 were involved in the interactions with the aromatic skeleton too (−6.3 kcal/mol). Ile281 contributed with −3.4 kcal/mol to the enthalpy term, mainly due to the strong H-bond between the NH substituent of compound **9** and Ile281 backbone oxygen. That H-bond was identified during more than 80% of the simulation time. Moreover, a stable water molecule was identified and found to be involved in the interactions at a position similar to that seen in most of the available crystal structures. It should be mentioned that a negative electrostatic contribution of Arg286 was identified (data not shown) that only marginally influenced the total free energy of binding, and might be considered for compound **9** hit optimization.

Finally, Cys285, Ile326, Tyr327, and Leu330 were involved in interactions (enthalpy contribution) with the central aromatic ring of compound **9** by total of −7 kcal/mol. The O-Ph-F ring interacted mainly with Arg288, Ser289, and Ile326 contributing with another −8 kcal/mol.

Adipocyte Differentiation. The adipogenic potential of the six transcriptional active PPARγ ligands was evaluated in an *in vitro* differentiation system applying dexamethazone treatment of the well-described 3T3-L1 preadipocyte cell line. Whereas vehicle treated cells differentiate poorly (less than 5% differentiating cells), addition of a full PPARγ agonist (Rosiglitazone) leads to almost complete adipocyte conversion (>90% differentiation) when analyzed by Oil Red O (ORO) staining (data not shown), quantification of AdipoRed staining (Table 2), or qPCR analysis of adipocyte marker genes (Table

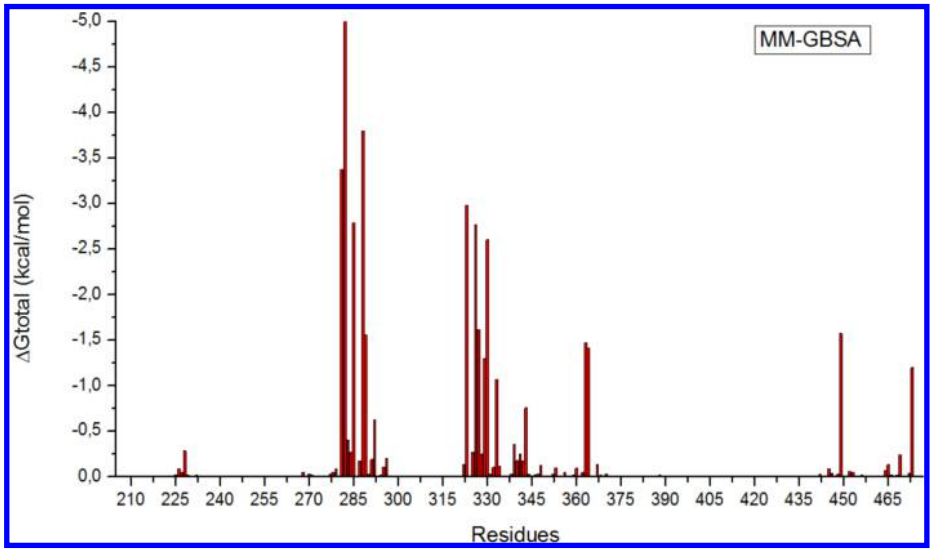

Figure 6. Contribution of the individual protein residues of PPARγ to the total binding free energy of compound **9** in complex with PPARγ, calculated by the MM-GBSA free energy decomposition method.

dx.doi.org/10.1021/ci3006148 | J. Chem. Inf. Model. 2013, 53, 923−937

Table 2. Induction of Adipocyte Differentiation[a]

	adipocyte differentiation		
		gene expression	
compound	AdipoRed Stain	FABP4	PPARγ2
2	0.5	0.7	0.6
5	15.9	7.0	7.3
9	5.2	3.2	2.9
12	9.0	2.9	2.6
15	1.5	1.1	0.4
17	3.0	0.9	1.1
Rosiglitazone	22.8	8.5	7.5

[a]Transcriptional active ligands were analyzed for their ability to stimulate adipocyte conversion of 3T3-L1 cells. Compounds were tested at the same concentration as in the transactivation assay (compound **9** up to 10 μM, compounds **2**, **12**, **15**, and **17** up to 50 μM and compound **5** up to 100 μM). Accumulated triglyceride was stained by AdipoRed and fluorescence quantified. Expression of genetic markers of differentiation (FABP4 and PPARγ2) was analyzed by qPCR. Triglyceride accumulation and marker gene expression is depicted relative to the DMSO vehicle values.

2). Reflecting the full agonist binding mode observed when docking compounds **5** and **12**, both induce adipocyte differentiation as measured by ORO (data not shown), AdipoRed stains, or expression of marker genes (Table 2). Compounds **2**, **12**, and **17** did not, and compound **9** only moderately enhanced adipocyte conversion (Table 2 and data not shown) supporting the docking studies that revealed partial agonist binding properties for these compounds. However, we cannot exclude that these compounds' low potential to induce adipocyte differentiation is caused by the inability to reach saturating compound concentration in the assay.

Selectivity Analysis of PPAR Binding. *PPARα.* (Figure 7) As one can expect the binding modes of the compounds in PPARα were similar to those in PPARγ, in agreement to what has been previously observed for a GW409544 PPARα/γ complex[19] and for many other ligands. However, the substitution of His323 with tyrosin in PPARα (Tyr314 in PPARα) had an impact on the coordination and the interactions between the ligands and the key protein residues. The histidine residue, His323 in PPARγ, might have significant impact on the binding of compound **9**, according to the above MD results, and for the ligand–protein interactions of the other compounds in our set. The docking study of compound **9** in PPARα showed that the molecule could reach some of the armI residues, formed by Tyr464, Tyr314, Ser280, and His440, but interacted only with His440, and no H-bonds were detected.

A similar observation was made for compound **2**. It has been already shown that PPARα has a larger, more hydrophobic and less polar binding pocket compared to PPARγ. The higher polarity of armI might prevent the molecule from forming a stable complex in this pocket. Compound **5** showed positive transactivation with PPARα. The molecule exhibited reasonable H-bond interactions between the sulfonyl group and Ser280 as well as between the amine group and Thr279. It was also in quite close contact to His440 and Tyr314. The observations from the docking studies support the experimental result.

Compound **12** displayed H-bond interactions with Ser280, Tyr314, and Tyr464 in the armI pocket but no contact with His440. The remaining part of the molecule was stabilized with hydrophobic contacts. Thus based on the docking result one can expect that this ligand would be active against PPARα too. However, no PPARα activity was measured for compound **12** (see Table S1 in the Supporting Information). It should be noted that there were differences in the interactions described above and those observed in PPARγ, where the contact with Phe273 of PPARα seemingly provoked a significant conformational change in the alkyl chain that might have impact on the activity.

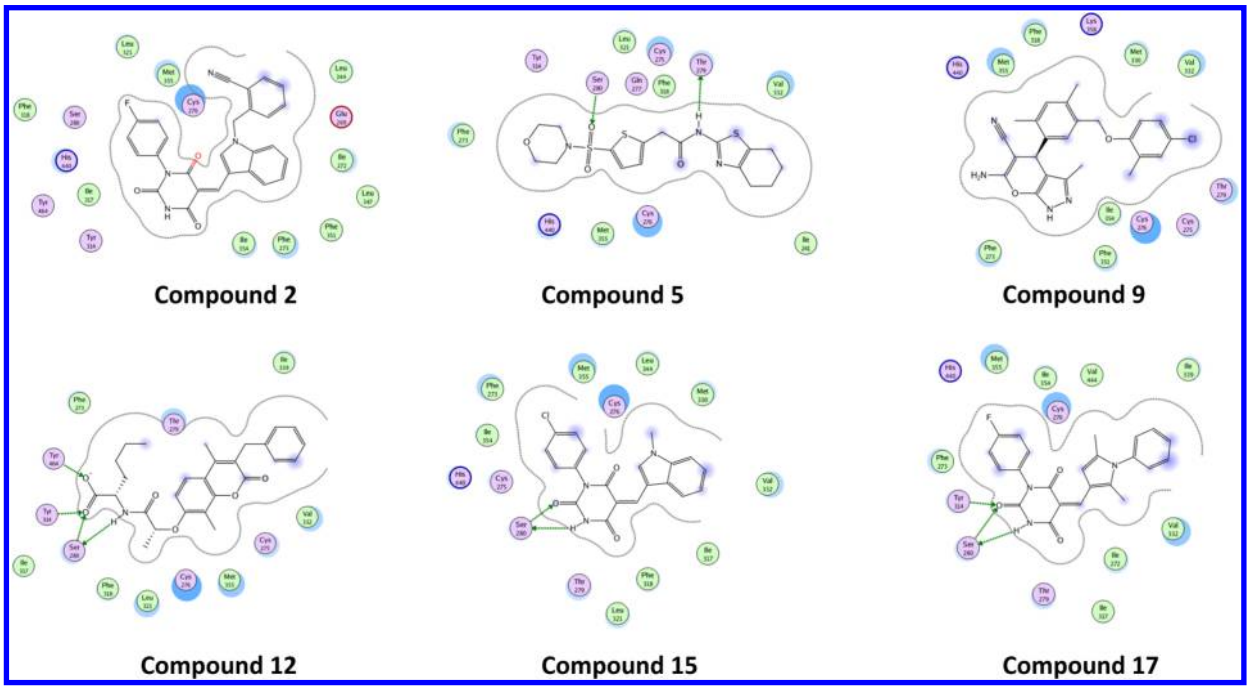

Figure 7. 2D picture of ligand–protein interactions of the six hits in PPARα (1K7L). Hydrophobic residues are depicted in green ball. The magenta balls are polar residues. Hydrogen bonds are represented with arrows (green when it is a side chain of a residue involved and blue for backbone). The ligand exposure is represented with blue dots.

dx.doi.org/10.1021/ci3006148 | J. Chem. Inf. Model. 2013, 53, 923–937

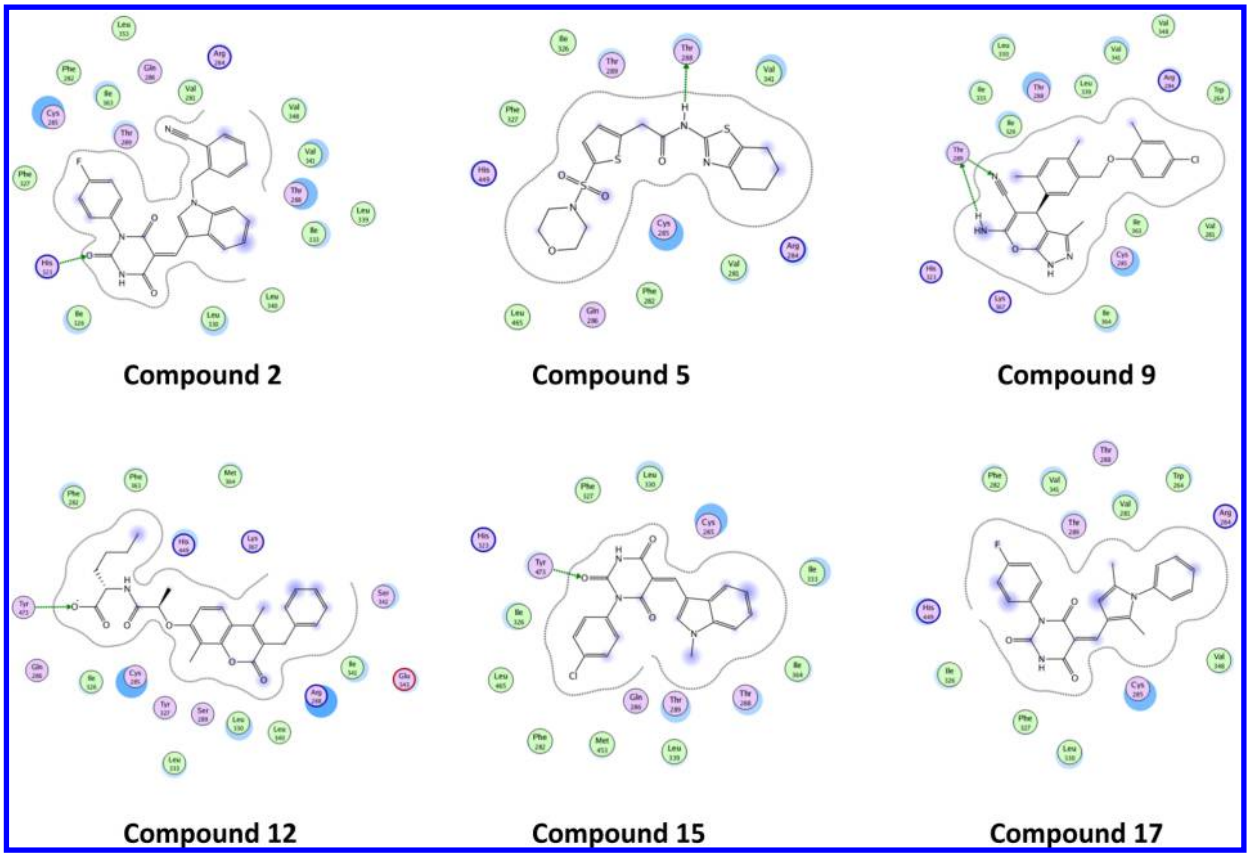

Figure 8. 2D picture of ligand–protein interactions of the six hits in PPARδ (1y0s). Hydrophobic residues are depicted in green ball. The magenta balls are polar residues. Hydrogen bonds are represented with arrows (green when it is a side chain of a residue involved and blue for backbone). The ligand exposure is represented with blue dots.

Both compounds **15** and **17** have identical binding mode in PPARα, as it was also in the case of PPARγ. Again due to the Phe273 conformation and the surrounding armIII residues, the barbituric groups were not able to reach His440 and Tyr464. Instead compound **15** formed only one H-bond with Ser280, and the indole group was located in the hydrophobic pocket. Compound **17** formed H-bond with both Ser280 and Tyr314, and similarly to compound **15**, it interacted with His440 only via the phenyl halogen. Hence, we expect these ligands to be either inactive or less active on PPARα compared with PPARγ, which is in agreement with the PPARα transactivation measurement (Table S1).

In general the amino acid substitutions and consequent reorganization of the armIII residues was the main source for the PPARα binding mode shift of the studied molecules compared to PPARγ. As a consequence, the ligands' key substituents could not interact with armI residues. Exceptions to this are compounds **5** and **12**. Compound **5** showed transactivation in our experiment, but compound **12** did not. The absence of H-bonding interaction between most of the ligands and key residues in the armI pocket provides an explanation of the lack of transactivation activity. Most agonists form conserved H-bonds with the activation function helix (AF-2 helix) which, in turn, enhances the recruitment of coactivators.[21]

PPARδ. PPARδ (Figure 8) has a smaller binding pocket than both PPARα and PPARγ, especially in the area of the armI pocket. Considering the critical role of interactions with the residues in the area next to the AF2-helix with respect to activity, the smaller cavity within armI might explain the inactivity of most of the identified PPARγ agonists for PPARδ. The reorganization of the binding pocked mentioned above is mainly due to the substitution of Ile280 to Phe (Ile281 in PPARγ) and the conformation of Leu330. Thus PPARγ ligands with large side chains attached to the key interaction substituent are hindered to be in contact with the armI protein residues. Thus some of the PPARγ ligands cannot bind to PPARδ; an example of this is GW409544.[12]

The lack of a second tyrosin, which is present in PPARγ, in the group of the key residues has an impact on binding too. For example, the position of the carbonitrile group of compound **9** was different to the one observed in PPARγ, and no strong interactions with residues of the armI pocket were identified. Compound **9** made only H-bond with Thr289, and the remaining part of the aromatic skeleton was in contact with His323 and Lys367 (Figure 8). The chlorophenyl group showed few hydrophobic contacts, but interacted also with Arg284, which had negative influence on the activity, according to our MD calculations above. Similar behavior was observed for compound **2**, which formed an H-bond only with His323, and no other interactions with residues in armI were observed in the docking.

Compound **5** managed to be in a contact with His449 through the sulfonyl group, but no H-bonds were observed with the armI residues. Instead the amino group of the ligand formed an H-bond with Thr288, which cannot stabilize the complex sufficiently. No transactivation activity was measured for this molecule (Table S1).

Compound **12** depicted a hydrogen bond between the carboxyl group of the molecule and Tyr473. However the

dx.doi.org/10.1021/ci3006148 | J. Chem. Inf. Model. 2013, 53, 923–937

attached alkyl chain was not able to fit in the smaller PPARδ pocket, most likely due to restrictions posed by the Phe282 and Phe363 residues. This compound would not be expected to bind to PPARδ, which is in agreement with the experimental result (Table S1).

The barbituric acid scaffold of compound **15** fitted well into the key residues of armI and H-bond with Tyr473, and close contact with His323 was observed. The latter might explain the observed activity (Table S1). However the distance between the barbituric group in compound **17** and armI residues was larger, presumably due to the methyl group, and the molecule was not able to interact with the key protein residues in armI. Again, based on previous assumptions, we conclude that the presence of methyl groups plays a major role in the activity.

In general, most of the identified hits were able to fit into the PPARδ pocket in a way that resembles the PPARγ binding mode. However, with the exception of compound **15**, the differences in the conformation of the substituted residues restricted the ligands and hindered them to reach and interact with the key protein residues in armI.

Regulation of Gene Expression. Of the six compounds exhibiting PPARγ agonistic properties one compound was chosen for further gene expression analysis. Compound **9** was selected as the most interesting compound as it was potent, was a relatively poor inducer of adipocyte differentiation, and did not harbor any chemical entities associated with obvious pharmacological problems. As previously observed, treatment of 3T3-L1 adipocytes with the partial PPARγ agonist nTZDpa lead to only modest transcriptional regulation as compared to the full agonist Rosiglitazone (Figure 9A). Compound **9** transcriptional effects, although even less, were comparable to those of nTZDpa, suggesting compound **9** to be more functional related to the partial agonist. Likewise, depicting the gene expression in a Venn-diagram reveals compound **9** to share a larger proportion of controlled gene with the partial rather than the full PPARγ agonist (Figure 9B). However, although sharing some functional overlap with nTZDpa and Rosiglitazone, the gene regulatory profile is mainly unique. Interestingly, among the genes induced by all three compounds are *Pfkfb3* and *Pdk4* previously suggested to mediate part of the insulin-sensitizing effect of Rosiglitazone. Accordingly, compound **9** increased insulin-stimulated glucose uptake in 3T3-L1 adipocytes (data not shown).

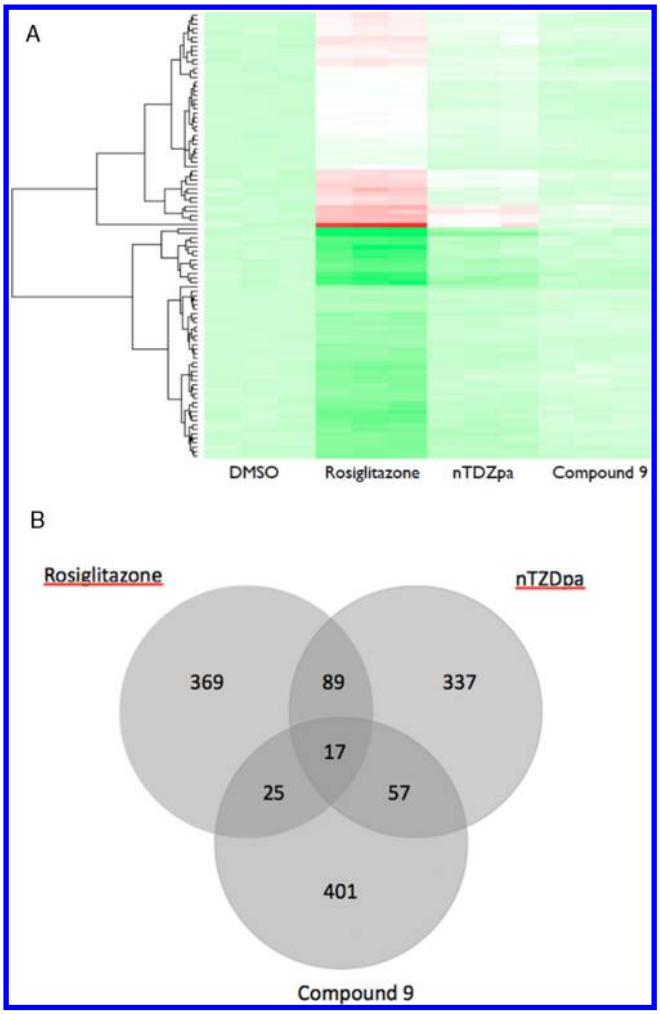

Figure 9. Gene expression differentiation between the control (DMSO, 0.1%) and the 3 compounds (Rosiglitazone (0.3 μM), nTZDpa (0.3 μM), and compound **9** (1 μM) (defined by a fold change in the range from −2 to 3.2). (A) Heatmap is constructed for the 100 most significantly differentially expressed genes. Green depicts down regulated genes and red upregulated genes. (B) Venn diagram of the 500 highest fold-change for Rosiglitazone, nTDZpa, and compound **9** and comparison between the common genes in the 3 samples.

CONCLUSION

We hereby applied an integrated *in silico*/*in vitro* workflow for the identification of novel PPARγ ligands with improved pharmacological properties compared to the existing drugs in the market. The pharmacophore-based virtual screening was performed on the ZINC library, and the identified 256 hits were further subjected to high throughput docking. 106 compounds that passed the docking filter were inspected visually, and 15 were selected based on the docking score, availability, structural diversity, and low or moderate risk of toxicity. Competitive binding and transactivation assay experiments on the 15 compounds showed that 11 of them were active against the PPARγ receptor, while six were also able to stimulate PPARγ-mediated transactivation. The high success rate among the compounds selected for testing shows that both the pharmacophore and docking models developed captured the key features important to ligand − protein binding.

The six hits were further tested for *in vitro* transactivation and *in silico* selectivity toward all three PPAR subtypes. Four of the hits (compounds **2**, **9**, **12**, and **17**) were found to be selective against PPARγ, and compounds **5** and **15** also showed transactivation toward PPARα and PPARδ, respectively. In addition, the docking results were applied to explain the mode of binding of the six identified ligands, and the binding mode of the most potent hit, compound **9**, was confirmed by MD simulation. The docking and MD results showed that the hits that were able to stimulate transactivation were in close contact and did form hydrogen bonds with the activation segment within the ligand binding domain of the respective PPAR forms. In cases where no transactivation was measured, close interaction with the activation segment through several hydrogen bonds was generally not achieved.

The most potent hit, compound **9**, was found to be a relatively poor inducer of adipocyte differentiation. Further studies on the transcriptional regulation properties of compound **9** revealed a gene regulatory profile that is to a large extent unique, however, functionally closer to this of a partial agonist. Compound **9** could, thus, serve as a novel lead

dx.doi.org/10.1021/ci3006148 | J. Chem. Inf. Model. 2013, 53, 923−937

compound for the development of the new generation of antidiabetic drugs. A novel functional group, the carbonitrile group, was identified to be a key substituent in the ligand–protein interactions. This particular finding illustrates the advantages of the combination of pharmacophore-based screening and docking in the identification of active compounds with novel structural features, embarking from known PPARγ agonist structures.

All in all, we believe that the applied workflow, which intertwines *in silico* and *in vitro steps*, is advantageous over more traditional strategies that keep separate the phases *of in vitro* experiments and model development, as it allows them to interchange information at various stages of the project and, thus, contribute actively to the decision making of one another.

Last but not least, we believe that the discovery of novel selective PPARγ ligands with partial agonist binding properties is a desired outcome not only because such compounds could be the new drug candidates for the treatment of type II diabetes but also because they constitute chemical probes for the elucidation of the biological function of PPARγ and its potential role in the treatment of other diseases e.g. obesity.

EXPERIMENTAL SECTION

Data Sets, Small Molecule Libraries, and Crystal Structures. The compound set employed in the pharmacophore model is given in Table S2. Virtual screening for PPARγ ligands was performed on the ZINC free database of commercially available compounds, version 7.[25] Almost 3 million unique structures in SD format from ZINC were imported into a database using Molecular Operating Environment (MOE).[26] These structures were washed, i.e. all inorganic compounds were removed and all ionizable groups were coordinated with neutral pH conditions. Energetically minimized conformations were generated using the MMFF94x force field, with a maximum number of conformers set to 250. For validation of the docking procedure and identification of a threshold value used in the docking screen, a data set of 19 PPARγ agonists with a broad range of transactivation values were assembled from the literature (see Table S3 in the Supporting Information). Cocrystallized structures of all three PPAR forms, -α, -δ, and -γ, including crystallographic data of their respective agonist were retrieved from the protein data bank (PDB), 1K7L, 1Y0S, and 1K74, respectively.

Pharmacophore Modeling. The ligand-based pharmacophore model was developed, refined, and evaluated using the pharmacophore elucidation application of the MOE software. The model was generated using the PPCH_All scheme, based on a compound set of seven PPARγ agonists and seven decoys. All agonists are selective to PPARγ; no dual or pan PPAR agonists were included. The set of actives was composed of the known antidiabetic drugs Rosiglitazone (TZD) and Farglitazar (non-TZD) and five other biologically relevant agonists with either full or partial binding properties. We made sure that the compounds covered a broad range of activities, from weak to medium and strong agonists. The decoys were manually selected from a set of the PPARγ inactive compounds that were structurally similar to the selected PPARγ agonists. Some of the selected decoys showed activity toward other targets of the nuclear receptor family. The pharmacophore was generated on the first aligned solution that was characterized by the best accuracy in separating actives from inactives. The pharmacophore model was then used for the virtual screening of the ZINC database of commercially available compounds. To be considered as a hit, the compound had to fit all the features of the pharmacophore.

Structure-Based Virtual Screening. The compounds that passed through the pharmacophore filter were subsequently evaluated with a docking screen performed with Autodock 4.1.[27] The following approach was adopted:

1) The 3D crystal structure of PPARγ in a complex with GW409544 (PDB code: 1K74) was used, where the ligand and water molecules were removed from the protein crystal structure. In all cases we performed a check and refined the quality of the used protein structures by the Schrödinger Protein Preparation Wizard. In particular, the structure with PDB ID: 1K74 showed some errors with respect to atom types and expected valence, but most of the indicated residues were at too long a distance from the ligand binding domain to affect the ligand binding. All these errors were solved by the above-mentioned tool prior to performing the virtual screening. Moreover, some of the residue side chain atoms were missing, mostly at the coactivator site, and were added by the Schrödinger Prime module.

2) In order to keep the degrees of freedom of the docking experiments on a manageable level and to avoid uncertainties caused by the use of many flexible residues, the docking was done with the rigid protein structure and flexible ligands. The ligand extracted from the PDB file was energy minimized and docked back into the crystal structure by the procedure described below.

3) The PDB structure used for the docking screen was chosen after a procedure in which all available crystal structures for PPARγ were retrieved from the PDB databank and prepared as described for 1K74 above. The seven cocrystallized PPARγ ligands from these crystal structures (1RDT (Faglitazar), 1GZY (Rosiglitazone), 2G0G, 2G0H, 1I71 (Tesaglitazar), and 1KNU) were consequently docked into each of the PPARγ crystal structures. The PDB structure, for which the docking best reproduced the binding mode of all the ligands (e.g., lowest RMSD between the docked and the measured structures), was chosen for the further docking screen.

The PDB structure chosen was 1K74. The sum of the RMSD values between the predicted pose of each of these seven ligands in PDB 1K74 and the corresponding experimentally established conformations were lower than 1.5 Å. The predicted and experimentally observed binding modes of Rosiglitazone and 2G0G are shown in Figure S1 in the Supporting Information.

4) Importantly, we performed a thorough analysis of all docking parameters that might influence the docking accuracy and thus created an individual "calibrated" Autodock docking protocol for the PPARγ receptor. Commonly, it has been reported that the grid size has an impact on Autodock accuracy, and different authors have optimized particularly this value in order to achieve a better performance. We extended here the optimization to include many other parameters as, for example, the Larmarckian genetic algorithm (LGA). Various combinations of the number of LGA energy evaluations and population size were explored, and the most successful were chosen. The influence of the rotation step of the flexible ligand bonds, initial ligand position in the binding pocket, and the grid coordinates were evaluated as well.

As mentioned above, the compounds were docked using the LGA algorithm. LGA describes the relationship between the protein and the ligand by the translation, orientation, and conformation of the ligand. Docking began with a population of

dx.doi.org/10.1021/ci3006148 | J. Chem. Inf. Model. 2013, 53, 923–937

random ligand conformations in random orientations and at random translations. Each docking experiment was derived from 100 different runs that were set to terminate after a maximum of 500,000 energy evaluations or 27,000 generations, yielding 100 docked conformations. The population size of the LGA algorithm was set to 50. The elitism number, the rate of gene mutation, and the rate of gene crossover were 1, 0.02, and 0.8, respectively. A pseudo-Solis and Wets local search was then used to minimize energy of the population. The probability that a docking solution in the population would undergo a local search was set to 0.06, and the constraint was set to a maximum of 300 iterations per search. The maximum numbers of successes or failures before changing the size of local search space (rho) were both set to 4. The starting conformations of each ligand were randomly selected. Translations of the compounds were set to have a maximum limit of 2 Å/step. Finally, we repeated the docking of the 256 compounds to the PPARγ receptor once more to ensure that the original docking poses were reproduced according to the process described above.

In order to identify an appropriate threshold for the docking screen, a test set of 19 known agonists with low to high transactivation values was collected from the literature (see Table S3 in the Supporting Information). Compounds with activity lower or equal to 10 μM ($-\log EC_{50} \geq 5$) were considered to be active, and compounds with activity higher than 10 μM were considered to be inactive. All 19 compounds were docked with the procedure described above, and the results were analyzed in order to implement a rationally based threshold value for the docking screen.

Knowledge Based Filtering. A subset of the compounds that passed through the docking screen was selected for experimental testing.

- Compounds containing chemical substructures with strong binding abilities, that were seen to be in close contact with key residues within armI in the PPARγ binding pocket, were represented in the set. This analysis was done by visual inspection of the binding modes of the docked ligands.

- Mostly compounds with relatively high docking scores were selected. In order to examine the applicability of using calculated docking scores as an indicator of receptor transactivation, a few compounds passing the docking screen with low and medium docking scores were also selected for experimental testing.

- In principal, we aimed to avoid highly toxic and/or reactive substructures, and the synthetic feasibility was also considered.

- It was ensured that the compounds chosen had appropriate structural diversity.

Competitive Binding Assay. IC_{50} values for respective compounds were determined by competitive binding using time-resolved fluorescence resonance energy transfer (LanthaScreen, Invitrogen) on a Victor2 microplate reader (PerkinElmer). Briefly, a terbium labeled anti-GST antibody was used to label purified GST-tagged PPARγ-LBD (ligand binding domain). Energy transfer from terbium to the tracer, a fluorescent pan PPAR agonist, enabled read-out of each test compound's ability to displace the tracer. RFU values from dose−response curves (triplicate sampling) for test compounds as well as positive controls (Rosiglitazone) were then analyzed using GraphPad Prism.[28] An unrestrained sigmoidal (one-binding site) dose−response curve was fitted to each data set by linear regression and allowing for determination of IC_{50} values. All compounds were tested in 10 different concentrations ranging from 3 nM to 500 μM (Rosiglitazone from 0.3 nM to 10 μM). Chemicals were obtained from Specs (compounds **1**, **9**, and **14**), Asinex (compound **2**), Enamine (compounds **3**, **5**, and **19**), Labotest (compound **4**), Chemical Block (compound **6**), Pharmeks (compounds **7** and **10**), and Early Discovery Chemistry (compounds **12**, **15**, **17**, and **18**) and were used without any further purification.

Nuclear Receptor-LBD Transactivation. Hepa1−6 cells were grown in minimum essential medium (MEM) (Gibco) supplemented with 10% FCS and antibiotics (62.5 μg/mL penicillin and 100 μg/mL Streptomycin). Mouse embryo fibroblasts (MEFs) were propagated in Dulbeccos Modified Eagle's Media (DMEM) supplemented with 10% fetal calf serum and antibiotics. Cells (Hepa1−6 were used for PPARα whereas MEFs were used for PPARγ, PPARδ, and RXRα transfections) were transfected in solution by Metafectene (Biontex) lipofection, essentially according to the manufacturer's instructions and seeded in media (MEM or DMEM) supplemented with 10% fetal calf serum and antibiotics in 96-well dishes at 24000 cells/cm^2. The transfection plasmid mix included the Gal4-responsive luciferase reporter, the expression vector for the fusion between the Gal4 DNA-binding domain and the nuclear receptor ligand binding domains, and a CMV-Renilla luciferase normalization vector (pRL-CMV, Promega). Six hours after addition of transfection mix to the cells, the media was changed to media (MEM or DMEM) supplemented with vehicle (0.1% DMSO), positive control (1 μM Rosiglitazone, 30 nM GW7647, 1 μM L165041, or 0.2 μM LG1069 for for PPARγ, PPARα, PPARδ, and RXRα, respectively), or compound. Approximately 18 hours later, cells were harvested, and lysates were analyzed for Photinus and Renilla luciferase activity by luminometry. All data points were performed in at least triplicate, and each sample was measured in duplicate. Luminometer raw data were analyzed in Microsoft Excel spreadsheets and presented as column graphs depicting average values of triplicates and including standard deviations.

Adipocyte Differentiation and Quantitative Real Time Polymerase Chain Reaction (qPCR). 3T3-L1 cells were grown in Dulbeccos modified Eagle's media (DMEM) supplemented with 10% calf serum and antibiotics (62.5 μg/mL penicillin and 100 μg/mL Streptomycin). The cells were seeded in 96-well plates (AdipoRed assay) or 6-well plates (gene expression) and grown to confluence. Two days post confluence (designated day 0) the cells were induced to differentiate with DMEM supplemented with 10% fetal bovine serum (FBS), antibiotics, 1 μM dexamethasone (Sigma), positive control (1 μM Rosiglitazone), vehicle (0.2% DMSO), or the compound tested. After 48 h, the cells were refed with DMEM supplemented with 10% FBS the positive control, vehicle, or the test compound. From day 4, medium contained DMEM with 10% FBS and antibiotics and were changed every second day until day 8. At day 8, accumulated triglyceride in 96-well seeded cells was quantified with an AdipoRed assay according to manufactures protocols. Briefly, cells were washed in PBS, directly stained with AdipoRed (Lonza), and fluorescence (excitation at 485 nm and emission at 572 nm) measured on a Victor2 microplate reader (PerkinElmer). All testing were performed at least twice in 3 concentrations with 8 replicates. Likewise, at day 8 RNA from 6-well plates was harvested, cDNA was synthesized, and the expression of adipocyte marker genes was analyzed on a mx3000 qPCR instrument (Stratagene).

dx.doi.org/10.1021/ci3006148 | J. Chem. Inf. Model. 2013, 53, 923−937

Selectivity Analysis. In order to rationalize the potential ligand−protein interactions involved in the PPAR binding and to further evaluate the selectivity of the identified hits toward all three PPAR forms *in silico*, a second docking screen was implemented. In addition to the 1K74 crystal structure that was selected for the docking screen for PPARγ, the crystal structures 1K7L for PPARα and 1y0s for PPARδ were used for docking of the six hits that showed transactivation in our experiment (Table 1). The docking was done with Autodock 4.1, using the method described in the Structure-based Virtual Screening section.

For validation, the ligands of the cocrystallized PDB complexes were redocked into the respective crystal structures. For 1K7L, the GW409544 ligand was docked to the same position compared to the conformation of the ligand's crystallized form. Thus, interactions with S280, Tyr314, Tyr464, and His440 in armI were reproduced in the docking. For 1y0s, the phenoxy-2-methylbutanoic acid part of ligand (GW2331) did bind to His449, Tyr473, and His323 in armI. The ligand pose matched entirely with the experimentally observed conformation of the ligand in the protein−ligand complex. For 1K74 and its ligand (GW409544) the interactions with Tyr473, His323, His449, and Ser289 were reproduced by the docking. The oxazol group shifted the position of O and N but was still located in the region of armII. The phenyl propyl amino group of the molecule was located within the armIII as expected.

Molecular Dynamics and Free Energy Calculations. *Molecular dynamics.* MD computations were carried out using the Amber 11 suite of programs[29] and the Amber99SB force field. As input structures we used those obtained from the docking analysis. A truncated octahedral box of TIP3 water molecules of 10 Å dimension and counterions were added to obtain the final solvated system. Initially, the systems were minimized for 5 000 steps. After initial 50-ps gradual heating from 0 to 300 K in NVT ensemble and 3 ns equilibration, a 10 ns-long production run in NPT ensemble was employed. Temperature regulation was carried out with a Langevin thermostat with collision frequency of 2 ps^{-1}. The time step of the simulations was 2 fs with a nonbonded cutoff of 9 Å using the SHAKE algorithm[30] and the PME method.[31] We used the backbone atoms of the protein and all heavy atoms of the ligand to evaluate RMSD of the ligand in complex with PPARγ-ligand and of the ligand alone. We used the first frame of the production run, and not the equilibration step, as a starting conformation for evaluating the RMSD. Therefore an initial value larger than zero can be expected for the RMSD.

Free Energy Calculations. Binding free energies of all systems were analyzed using the MM-PBSA (Molecular Mechanics Poisson−Boltzmann/Surface Area) approach within the Amber 11 suite. The binding free energies (ΔG_{bind}) were computed as

$$\Delta G_{bind} = G_{complex} - (G_{protein} + G_{ligand}) \quad (1)$$

$$\Delta G_{bind} = \Delta G_{gas} + \Delta G_{solv} - T\Delta S \quad (2)$$

$$\Delta G_{gas} = \Delta G_{ele} + \Delta G_{vdw} \quad (3)$$

$$\Delta G_{solv} = \Delta G_{PB} + \Delta G_{nonpolar} \quad (4)$$

$$\Delta G_{nonpolar} = \gamma A + b \quad (5)$$

The sum of the molecular mechanical energies, ΔG_{gas}, was divided into contributions from the electrostatic potential (ΔG_{ele}) and the van der Waals (ΔG_{vdw}) potential. The solvation free energy (ΔG_{solv}) is composed of two parts: a polar solvation free energy (ΔG_{PB}) and a nonpolar solvation free energy ($\Delta G_{nonpolar}$). All energies are averaged along the MD trajectories. Both, the single and multiple trajectory approach were applied to estimate the energies. For the multiple trajectory approach we used the 10 ns MD simulations of individual protein complexes, but as a result the standard errors were almost 17 times larger than those obtained with the single trajectory approach. Thus, only the data from the single trajectory approach were reported, because the estimation of energies in this manner has proven to be successful. The reason for the success of this approach is the cancellation of errors that hides the effect of incomplete sampling. The snapshots of each system were sampled from the last 5 ns single trajectory with an interval of 10 ps, i.e. 500 snapshots. ΔG_{gas} was obtained using Amber 11 sander module, and estimation of ΔG_{PB} was conducted with a built-in module PBSA in Amber 11. $G_{nopolar}$ was determined from eq 5, where A is the solvent-accessible surface area estimated using the Molsurf program, which is a part of the Amber 11 suite programs, using a solvent probe radius of 1.4 Å. γ and b are empirical constants set to 0.0072 kcal mol^{-1} $Å^{-2}$ and 0.92 kcal/mol, respectively. To assess the $T\Delta S$ term in eq 2 the conformational entropy was calculated using 50 frames averaged along the MD trajectory and normal mode (Nmode) analysis by the Amber 11 package. The enthalpy contribution of the protein residues to the binding was evaluated by MM-GBSA decomposition approach. The entropy term was neglected in these calculations.

Gene Expression Analysis. 3T3-L1 cells were grown in Dulbeccos modified Eagle's media (DMEM) supplemented with 10% calf serum and antibiotics (62.5 μg/mL penicillin and 100 μg/mL Streptomycin). The cells were seeded in 6-well plates and grown to confluence. Two days postconfluence (designated day 0) the cells were induced to differentiate with DMEM supplemented with 10% fetal bovine serum (FBS), antibiotics, 1 μM dexamethasone (Sigma), 0.5 mM isobutylmethylxanthine (Aldrich), and 1 μg/mL insulin (Sigma). After 48 h, the cells were reefed with DMEM supplemented with 10% FBS and 1 μg/mL insulin. From day 4, medium contained DMEM with 10% FBS and antibiotics and were changed every second day until day 8. At day 8, medium was changed to include vehicle (0.1% DMSO), positive controls (0.3 μM Rosiglitazone and 0.3 μM nTZDpa), or the compound **9** (1 μM). Twenty-four hours later RNA was harvested.

Microarray Analysis. Global gene expression was analyzed using GeneChip Mouse Gene 1.0 ST Arrays (Affymetrix). In brief, sense-strand cDNA was synthesized using the Ambion WT Expression kit (Ambion), cDNA fragmentation and labeling were performed using the GeneChip WT Terminal labeling kit (Affymetrix), and hybridization and wash were performed using the GeneChip Hybridization Wash and Stain Kit (Affymetrix). All steps were performed as described by the manufacturer.

■ ASSOCIATED CONTENT

Ⓢ Supporting Information

Compound set used for the generation of the ligand-based pharmacophore model; training set of compounds for validation of docking; nuclear receptor selectivity of hit compounds; 2D picture of ligand−protein interactions of the

dx.doi.org/10.1021/ci3006148 | J. Chem. Inf. Model. 2013, 53, 923−937

six hits in PPARγ; RMSD of PPARy in a complex with compound **9** during the MD simulation; PPARy B-factors calculated by MD analysis. This material is available free of charge via the Internet at http://pubs.acs.org.

AUTHOR INFORMATION

Corresponding Author

*Phone: +45 45256162. Fax: +45 45931585. E-mail: irene@cbs.dtu.dk (I.K.). Phone: +45 35324443. E-mail: kk@bio.ku.dk (K.K.).

Author Contributions

I.K., R.K.P., F.F., and O.T. contributed equally to this work.

Notes

The authors declare no competing financial interest.

ACKNOWLEDGMENTS

I.K. and S.O.J. acknowledge grants from the Danish Research Council for Technology and Production Sciences (FTP), and T.O. acknowledges a guest professorship given by FTP as well. I.K., S.O.J., O.T., and F.F. thank the NABIIT program under the Danish Strategic Research Council for financial support, including a specific grant given under the SVM program to promote industrial-academic collaboration. T.E.N. is grateful to the Lundbeck Foundation, the Torkil Holm Foundation, and the DSF Center for Antimicrobial Research for financial support.

ABBREVIATIONS USED

PPAR, peroxisome proliferator-activated receptor; TZDs, thiazolidinediones; VS, virtual screening; PDB, protein data bank; CN, carbonitrile; SO_2, sulfonyl; MD, molecular dynamics; ORO, Oil Red O; MOE, molecular operating environment; LGA, Larmarckian genetic algorithm; LBD, ligand binding domain; MEM, minimum essential medium; MEFs, mouse embryo fibroblasts; DMEM, Dulbeccos Modified Eagle's Media; qPCR, quantitative real time polymerase chain reaction; FBS, fetal bovine serum; MM-PBSA, Molecular Mechanics Poisson−Boltzmann/Surface Area

REFERENCES

(1) Goebel, M.; Staels, B.; Unger, T.; Kintscher, U.; Gust, R. Characterization of new PPARgamma agonists: benzimidazole derivatives - the importance of position 2. *ChemMedChem* **2009**, *4*, 1136−1142.

(2) Willson, T.; Lambert, M.; Kliewer, S. Peroxisome proliferator−activated receptor γ and metabolic disease. *Annu. Rev. Biochem.* **2001**, *70*, 341−367.

(3) Semple, R.; Chatterjee, V.; O'Rahilly, S. PPARγ and human metabolic disease. *J. Clin. Invest.* **2006**, *116*, 581−589.

(4) Higgins, L. S.; Mantzoros, C. S. The development of INT131 as a selective PPARgamma modulator: Approach to a safer insulin sensitizer. *PPAR Res.* **2008**, 936906.

(5) Kliewer, S. A.; Sundseth, S. S.; Jones, S. A.; Brown, P. J.; Wisely, G. B.; Koble, C. S.; Devchand, P.; Wahli, W.; Willson, T. M.; Lenhard, J. M.; Lehmann, J. M. Fatty acids and eicosanoids regulate gene expression through direct interactions with peroxisome proliferator-activated receptors alpha and gamma. *Proc. Natl. Acad. Sci. U.S.A.* **1997**, *94*, 4318−4323.

(6) Elte, J.; Blicklé, J. Thiazolidinediones for the treatment of type 2 diabetes. *Eur. J. Intern. Med.* **2007**, *18*, 18−25.

(7) Guan, Y.; Hao, C.; Cha, D.; Rao, R.; Lu, W.; Kohan, D.; Magnuson, M.; Redha, R.; Zhang, Y.; Breyer, M. Thiazolidinediones expand body fluid volume through pparγ stimulation of enac-mediated renal salt absorption. *Nat. Med.* **2005**, *11*, 861−866.

(8) Pan, H.; Lin, Y.; Chen, Y.; Vance, D.; Leiter, E. Adverse hepatic and cardiac responses to rosiglitazone in a new mouse model of type 2 diabetes: Relation to dysregulated phosphatidylcholine metabolism. *Vasc. Pharmacol.* **2006**, *45*, 65−71.

(9) Liu, K.; Lambert, M.; Leesnitzer, L.; W Oliver, J.; Ott, R.; Plunket, K.; Stuart, L.; Brown, P.; Willson, T.; Sternbach, D. Identification of a series of PPARγ/δ dual agonists via solid-Phase parallel synthesis. *Bioorg. Med. Chem. Lett.* **2001**, *11*, 2929−2962.

(10) Lin, C.; Peng, Y.; Coumar, M.; Chittimalla, S.; Liao, C.; Lyn, P.; Huang, C.; Lien, T.; Lin, W.; Hsu, J.; Cheng, J.; Chen, X.; Wu, J.; Chao, Y.; Lee, H.; Juo, C.; Wu, S.; Hsieh, H. Design and structural analysis of novel pharmacophores for potent and selective peroxisome proliferator-activated receptor gamma agonists. *J. Med. Chem.* **2009**, *52*, 2618−2622.

(11) Knouff, C.; Auwerx, J. Peroxisome proliferator-activated receptor-gamma calls for activation in moderation: lessons from genetics and pharmacology. *Endocr. Rev.* **2004**, *25*, 899−918.

(12) Bruning, J. B.; Chalmers, M. J.; Prasad, S.; Busby, S. A.; Kamenecka, T. M.; He, Y.; Nettles, K. W.; Griffin, P. R. Partial agonists activate PPARgamma using a helix 12 independent mechanism. *Structure* **2007**, *15*, 1258−1271.

(13) Lu, I.-L.; Huang, C.-F.; Peng, Y.-H.; Lin, Y.-T.; Hsieh, H.-P.; Chen, C.-T.; Lien, T.-W.; Lee, H.-J.; Mahindroo, N.; Prakash, E.; Yueh, A.; Chen, H.-Y.; Goparaju, C. M. V.; Chen, X.; Liao, C.-C.; Chao, Y.-S.; Hsu, J. T.-A.; Wu, S.-Y. Structure-based drug design of a novel family of PPARgamma partial agonists: virtual screening, X-ray crystallography, and in vitro/in vivo biological activities. *J. Med. Chem.* **2006**, *49*, 2703−2712.

(14) Henriksen, K.; Byrjalsen, I.; Qvist, P.; Beck-Nielsen, H.; Hansen, G.; Riis, B. J.; Perrild, H.; Svendsen, O. L.; Gram, J.; Karsdal, M. A.; Christiansen, C. Efficacy and safety of the PPARγ partial agonist balaglitazone compared with pioglitazone and placebo: a phase III, randomized, parallel-group study in patients with type 2 diabetes on stable insulin therapy. *Diabetes Metab. Res. Rev.* **2011**, *27*, 392−401.

(15) Hwang, J.; Lee, M.; Kim, H.; Sung, M.; Kim, H.; Kim, M.; Kwon, D. Antiobesity effect of ginsenoside Rg3 involves the AMPK and PPARg signal pathways. *Phytother. Res.* **2008**, *23*, 262−266.

(16) Berman, H. M.; Westbrook, J.; Feng, Z.; Gilliland, G.; Bhat, T. N.; Weissig, H.; Shindyalov, I. N.; Bourne, P. E. The Protein Data Bank. *Nucleic Acids Res.* **2000**, *28*, 235−242.

(17) Li, Y.; Choi, M.; Suino, K.; Kovach, A.; Daugherty, J.; Kliewer, S. A.; Xu, H. E. PDB ID: 1ZGY Structural and biochemical basis for selective repression of the orphan nuclear receptor liver receptor homolog 1 by small heterodimer partner. *Proc. Natl. Acad. Sci. U.S.A.* **2005**, *102*, 9505−9510.

(18) Nolte, R. T. PDB ID: 2PRG Ligand binding and co-activator assembly of the peroxisome proliferator-activated receptor-gamma. *Nature* **1998**, *395*, 137−143.

(19) Xu, H. E. Structural determinants of ligand binding selectivity between the peroxisome proliferator-activated receptors. *Proc. Natl. Acad. Sci. U.S.A.* **2001**, *98*, 13919−13924.

(20) Mahindroo, N. PDB ID: 2F4B Indol-1-yl acetic acids as peroxisome proliferator-activated receptor agonists: Design, synthesis, structural biology, and molecular docking studies. *J. Med. Chem.* **2006**, *49*, 1212−1216.

(21) Markt, P.; Schuster, D.; Kirchmair, J.; Laggner, C.; Langer, T. Pharmacophore modeling and parallel screening for PPAR ligands. *J. Comput.-Aided. Mol. Des.* **2007**, *21*, 575−590.

(22) Lehmann, J. M.; Moore, L. B.; Smith-Oliver, T. A.; Wilkison, W. O.; Willson, T. M.; Kliewer, S. A. An antidiabetic thiazolidinedione is a high affinity ligand for peroxisome proliferator-activated receptor gamma (PPAR gamma). *J. Biol. Chem.* **1995**, *270*, 12953−12956.

(23) Plewczynski, D.; Łaźniewski, M.; Augustyniak, R.; Ginalski, K. Can we trust docking results? Evaluation of seven commonly used programs on PDBbind database. *J. Comput. Chem.* **2011**, *32*, 742−755.

(24) Sundriyal, S.; Viswanad, B.; Ramarao, P.; Chakraborti, A.; Bharatam, P. New PPARgamma ligands based on barbituric acid: virtual screening, synthesis and receptor binding studies. *Bioorg. Med. Chem. Lett.* **2008**, *18*, 3192−3195.

(25) Irwin, J. J.; Shoichet, B. K. A free database of commercially available compounds for virtual screening. *J. Chem. Inf. Mod.* **2005**, *45*, 177−182.
(26) MOE: *Molecular Operating Environment, version 2007.09*; Chemical Computing Group Inc.: Montreal, QC, Canada, 2008.
(27) Morris, G. M.; Goodsell, D. S.; Halliday, R. S.; Huey, R.; Hart, W. E.; Belew, R. K.; Olson, A. J. Automated docking using a Lamarckian genetic algorithm and an empirical binding free energy function. *J. Comput. Chem.* **1998**, *19*, 1639−1662.
(28) *GraphPad Prism*; GraphPad Software: http://www.graphpad.com/scientific-software/prism/GraphPadPrism (accessed November 22, 2012).
(29) Case, D.; Darden, T.; Cheatham, T.; Simmerling, C.; Wang, J.; Duke, R.; Luo, R.; Walker, R. C.; Zhang, W.; Merz, K.; Roberts, B.; Hayik, S.; Roitberg, A.; Seabra, G.; Swails, J.; Goetz, A.; Kolossváry, I.; Wong, K.; Paesani, F.; Vanicek, J.; Wolf, R.; Liu, J.; Wu, X.; Brozell, S.; Steinbrecher, T.; Gohlke, H.; Cai, Q.; Ye, X.; Wang, J.; Hsieh, M.; Cui, G.; Roe, D.; Mathews, D.; Seetin, M.; Salomon-Ferrer, R.; Sagui, C.; Babin, V.; Luchko, T.; Gusarov, S.; Kovalenko, A.; Kollman, P. *AMBER 11*; University of California, San Francisco.
(30) Ryckaert, J.-P.; Ciccotti, G.; Berendsen, H. J. . Numerical integration of the cartesian equations of motion of a system with constraints: molecular dynamics of n-alkanes. *J. Comput. Phys.* **1977**, *23*, 327−341.
(31) Petersen, H. G. Accuracy and efficiency of the particle mesh Ewald method. *J. Chem. Phys.* **1995**, *103*, 3668−3679.